Submitted to ADVANCED MATERIALS

DOI: 10.1002/adma.((please add manuscript number))

# Tunable complete optical absorption in multilayer structures including $Ge_2Sb_2Te_5$ without lithographic patterns

*Vahagn K. Mkhitaryan, Dhriti S. Ghosh, Miquel Rudé, Josep Canet-Ferrer, Rinu Abraham Maniyara, Kavitha K. Gopalan and Valerio Pruneri**

[*] V. K. Mkhitaryan, Dr. D. S. Ghosh, M. Rudé, Dr. J. Canet-Ferrer, R. Abraham Maniyara, K. K. Gopalan, Corresponding-Author, Prof. V. Pruneri
ICFO-Institut de Ciencies Fotoniques,
The Barcelona Institute of Science and Technology
08860 Castelldefels, Spain
E-mail: valerio.pruneri@icfo.eu
Prof. V. Pruneri
ICREA-Institució Catalana de Recerca i Estudis Avançats
Passeig Lluís Companys, 23
08010 Barcelona, Spain

Keywords: phase change materials, perfect absorber, broadband, angle independent, polarization independent

Controlling the spectral transmission, reflection, and absorption properties of optical structures is of great interest for many applications in photonics. Particularly, perfect absorbers over a wide frequency (wavelength) range are desirable for thin-film thermal emitters, thermo-solar cells, photodetectors and smart windows. Up to date, several mechanisms have been proposed to achieve nearly 100% absorption in various frequency ranges of the electromagnetic spectrum; starting from microwaves to near infrared (NIR) and visible. One of the first demonstrations of a structure that was absorbing with nearly 100% efficiency was proposed by Landy et al. in 2008,[1] where metamaterial resonator arrays were used to achieve narrowband and highly resonant absorption of GHz and THz waves. The narrowband character of the resonances can be an advantage when absorbers with high quality factor are required and wavelength selectivity is desirable. However there are many applications that need broadband absorption. To this end great efforts have been made during the last decade, for instance by mixing multiple resonances in a many-fold resonator, which can lead to, e.g. dual band[2] or multiband[3-9] resonant absorption. Unfortunately fabrication of these structures requires

sophisticated techniques such as micro- or nano-lithography, severely limiting their scalability and increasing the cost of the absorber.

One promising lithography-free approach is the use of absorbers that take advantage of the strong interference effects arising in few layer hetero-structures. Several proposals demonstrated perfect absorption in metal-dielectric-metal Fabry-Perot-like structures, both in the narrowband[10] and broadband regimes.[11, 12] In these structures a dielectric layer is placed in between a bottom metallic mirror and a top semitransparent mirror, forming an optical cavity where the light is confined and gradually absorbed by the metallic layers. Other configurations with similar designs but using periodic[13, 14] or random arrays[15-17] of nanoparticles as a top mirror layer were also experimentally demonstrated. In all these structures the light power was converted into heat due to absorption in the metallic layers or in metallic particles. However, after conversion of light into heat cannot be exploited by photodetectors or photovoltaic cells. In this case light should be absorbed by the active semiconductor layer where the creation of electron-hole pairs takes place. High absorption in thin semiconductor layers over a broad range of wavelengths[18-20] has been demonstrated using a few nm thick Ge layer deposited on the surface of an Au mirror. In this case the absorption enhancement is due to strong interference effects due to the phase accumulation when light passes through this absorbing layer, causing destructive interference on the top surface of the structure and leading to reflection cancelation, which enhances the absorption at the same time. This reflection suppression mechanism is similar to that taking place in $\lambda/4$ layers, where a $\pi$ phase shift occurs between primary and partially reflected light beams. The only difference here is that the $\pi$ phase shifts can be achieved with much thinner layers due to stronger phase accumulation in an absorbing layer with respect to their dielectric (non-absorbing) counterparts.

Recently, tunable perfect absorbers have been demonstrated using patterned graphene,[21,22] or dye molecules.[23] Another approach consists of using the strong optical interference effects in

phase change material (PCM) layers to achieve high absorption.[24] PCMs exhibit two or more stable structural phases and can undergo reversible phase transitions between these states under external excitations, which can be either thermal, electrical or optical. During phase transitions, PCMs significantly change their optical, electrical and thermal properties, which makes them attractive in many applications, ranging from data storage to tunable optical components. In recent years two of the most known phase change materials $VO_2$[25] and $Ge_2Sb_2Te_5$(GST) have been shown to be promising candidates to design reconfigurable optical devices.[26-29] Particularly they were used in combination with plasmonic structures to tune or control their optical properties.[27-30] These tuning effects are based on the fact that plasmonic resonances are very sensitive to changes in the dielectric function of the surrounding PCM. For practical purposes, GST is considered to be more promising since it preserves its phase even after removal of the external excitations. GST layers have also been proposed as a suitable material for tunable perfect absorber designs both in the narrowband mode[30] and in the broadband mode,[31-34] for instance by depositing metallic nanoantenna arrays on top of them. They thus required time consuming and expensive lithography techniques.

In this paper, we propose a lithography-free few-layer perfect absorber based on a combination of GST and readily available metallic and dielectric materials. More specifically, we demonstrate two perfect absorber designs: a broadband perfect absorber in the visible and a narrowband resonant absorber in the NIR. GST plays a crucial role in both achieving a large absorption and enabling tunable response by phase transition. Besides being easy to fabricate and inexpensive, the layered design allows a wide range of possible combinations of metals and dielectrics with GST without constraints to the optical response. We also introduce a simulation tool based on the transfer matrix together with a genetic algorithm that is used to maximize the absorption in a given structure, and compare with the multiple alternatives available. Among the successful algorithm outputs, we choose the simplest two structures, consisting of few layers

and noted that more complicated multilayer geometries cannot offer noticeable improvements (in terms of absorption and tunability).

A schematic of the broadband perfect absorber in the visible range is shown in **Figure 1**a. The 4 layer structure was deposited on fused silica substrate. A 100 nm thick metal layer on the bottom acts as a reflector in our structure, followed by a thin (20nm) $SiO_2$ spacer layer which separates the 13 nm GST layer from the mirror. Another 60 nm thick $SiO_2$ layer is deposited on top of GST, acting as an index matching layer between air and the rest of the structure, and, at the same time, protecting the GST film from oxidation. The thickness of each layer was optimized to achieve maximum absorption in the visible range using simulations based on a transfer matrix algorithm. This was achieved by fixing the thicknesses of the mirror and GST layers and then calculating the average absorption over the visible range versus the thicknesses of the top and spacer $SiO_2$ layers (Figure 1b). Moreover we fabricated samples both with Au and the cheaper alternative Ni as mirror layers. Both of them have similar absorption spectra with slightly broader response in the latter case. This can be explained by the higher intrinsic losses of Ni compared to Au. The experimental absorption curves for the sample with Ni mirror are given in Figures 1c and d for the amorphous and crystalline GST phases, respectively. Both samples show nearly 100% absorption in the visible range when GST is in the amorphous phase, remaining above 80% up to 900 nm. Upon a phase transition from the amorphous to the crystalline phase, a 20% reduction of the absorption is observed uniformly over the entire band (Figure 1d). The changes were more pronounced for the reflection, which varied from 0% to 20%, making the effect clearly visible to the naked eye (insets of Figures 1c and d). Similar results are obtained using a Au mirror (see SI Figure 1).

The absorption mechanism can be attributed to strong absorption effects in the ultrathin semiconductor layers associated to interference between multiple reflected light beams.[18, 19] Here, due to the high refractive index of GST at these wavelengths light beams accumulate

strong phase shifts upon each passage through it and subsequent reflection from the metallic mirror surface. These partial beams interfere destructively with the primary reflected beam at the top surface of the GST layer if the relative phase difference is equal to $\pi$. It is worth pointing out that the $\pi$ shift difference is not the only condition to achieve zero reflection in the device. The sum of the reflected beams amplitude must be close to the amplitude of the primary beam. However, this may not be satisfied completely in the case of very absorptive active layers, as the amplitude of each partial wave will be very small due to "multiple reflections" attenuation. In our work the top index matching layer reduces the reflection and intensity of the primary beam at the first GST interface. In this way one can easily achieve complete destructive interference.

We performed simulations to find the thickness of the index matching $SiO_2$ layer for a given GST layer thickness that maximizes the average absorption over the whole visible range. The resulting color map plot is shown in Figure 1b, from which one can see that there exists a range of parameters that enhance the absorption. One of the main advantages of the proposed structure with thin absorbing layers is its omnidirectionality, i.e. the absorption remains high up to large angles of incidence. This is thanks to the fact that the structure is composed of very thin layers and that the internal angles of the refracted beams are small because of the high refractive index of GST, thus large angles are needed to move away from the destructive interference condition. **Figure 2**a and Figure 2b show a plot of the theoretical absorption as a function of incidence angle for p and s polarizations, respectively. Figure 2c and Figure 2d are the corresponding color-map plots of the absorption as a function of wavelength and incidence angle. The absorption remains high up to large incidence angles of about $70^o$. The insets of Figure 2a and Figure 2b show the calculated absorbed power distributions. It is interesting to note that most of the light (about 80%) is absorbed in the GST layer, making the proposed structure

particularly suitable for photovoltaic and photodetection applications where strong absorption in the semiconductor layer is required.

In order to better quantify the potential of our design we compared these results with the absorption of bare GST layers with different thicknesses on fused silica for both the crystalline and the amorphous phases (see SI Figure 2a and 2b). In this case the absorption of bare GST saturates for thicknesses above 75 nm and thus it can never exceed 60% (amorphous) and 40% (crystalline). This confirms the crucial role of the $SiO_2$ layer and interference effects in enhancing the overall absorption. These numerical simulations are also confirmed by measurements of GST films deposited under the same conditions (see SI Figure 2c and 2d).

Although the absorption efficiency and the bandwidth of the proposed structures in the visible is very high and a considerable amount of contrast can be achieved by changing the phase of the GST layer from amorphous to crystalline, an even stronger contrast (tuning) can be demonstrated in the NIR. This is because in the visible range both amorphous and crystalline GST are highly absorptive (see refractive indices of GST in Figure SI.7) limiting the absorption contrast upon transition from one state to another. On the contrary, in the NIR range the absorption of amorphous GST becomes negligible while this is not the case for crystalline GST. This in turn leads to a stronger tuning which can be achieved by a resonant absorber design, which, similarly to the visible counterpart, consists in a few layers. **Figure 3**a shows a schematic of the second structure proposed in this work. It consists of 4-layers with a configuration similar to the broadband case but with a 10 nm Au layer replacing the top $SiO_2$ layer. We considered two thicknesses for the $SiO_2$ spacer layer, which is another parameter providing design flexibility and optimization. For each thickness of the $SiO_2$ layer (50 and 100 nm) we investigated samples with 100 nm, 150 nm and 200 nm thick GST layers.

We have performed parametric sweep simulations demonstrating the dependence of the resonant wavelength on thickness change for both GST and $SiO_2$ layers. One of these

parametric sweep plots is shown in Figure 3b for a given $SiO_2$ layer thickness (100nm) and varying GST layer thickness (additional parametric sweep plots are shown in Figure S3). It is evident that for each GST layer thickness there exists a resonant wavelength at which nearly 100% absorption occurs, thus allowing one to design a perfect absorber for any desired wavelength by simply choosing such a thickness. The experimental absorption curves for the different thicknesses of GST and SiO2 layers are shown in Figures 3c and 3d. Contrary to the broadband nature of the first structure in the visible, this second structure shows resonant absorption in the NIR region with very high absorption efficiencies above 80% at the resonance wavelength in all cases. This experiment is also performed using Ni mirrors, showing similar narrowband behavior (see SI Figure S6). Moreover when the GST is crystallized these resonances are strongly reduced (down to 5%) and red shifted (Figure 3c and 3d), this is due to an increase in both the refractive index and the absorption coefficient in the NIR region of GST upon crystallization (Figure S8), which breaks the condition for Fabry-Pérot resonances which were present in the amorphous phase. These changes are more evident if one looks at the reflection spectra (R=1-A), which shows how the structure changes from a state of almost zero reflection to a state with high reflection (see SI Figure S7).

Although it will be shown below that the absorption mechanisms are different compared to the broadband case, the light trapping and Fabri-Pérot resonances are again attributed to reflection cancelation at the top surface of the structure. This can be easily demonstrated by means of the next equations (see SI for details):

$$|r_{12}| = \frac{|t_{12}t_{21}r_{2/5}|}{|1-r_{21}r_{2/5}e^{2i\beta_2 d_2}|} \quad (1)$$

$$arg(r_{12}) = arg(t_{12}t_{21}r_{2/5}) - arg(1 - r_{21}r_{2/5}e^{2i\beta_2 d_2}) + 2\beta_2 d_2 + \pi \quad (2)$$

that should be satisfied simultaneously in order to cancel the reflection at the top surface. Figure 3b shows the region of the parameter space where these two equation are satisfied simultaneously. As one can see both the maximal absorption regions and the balance equation

regions coincide. This shows that the described cancelation mechanism is responsible for the light trapping and enhanced absorption.

As in the case of the broadband absorber, in this case as well the absorption does not change significantly up to very large angles of incidence, confirming the role played by the high refractive index of GST in reducing the effects that one would expect when increasing the layer thickness. This can be seen in Figure S5 of SI where the experimental absorption curves for different samples are shown for different angles of incidence. It is worth noting that despite a similar architecture, the broadband and resonant absorbers mechanisms are different. As we have discussed above, in the former case the absorption is associated to destructive interference between reflected beams with most of the light absorbed in the GST layer. In the amorphous phase, GST is very absorbing in the visible while is very transparent in the NIR. On the contrary, in the crystalline phase it becomes more absorbing when one goes from the visible to NIR (see SI Figure S8). In this case the structure is a resonant (Fabry-Pérot like) structure where the absorption occurs mostly in the top and bottom metal layers. Since the quality factor of the resonances in the Fabry-Pérot like structures depend on that of the cavity (mirrors), we used Au for both the top and bottom mirrors because it is less absorptive than Ni. This provided narrower resonances in the near IR. Ni mirrors were preferred in the visible as their absorption was not critical and are less expensive than Au mirrors. The structure with Ni mirror and its performance are shown in Figure S6 of the supplementary information section.

We calculated the spatial distribution of the normalized absorbed power within the sample at three different wavelengths (**Figure 4**b, c and d), corresponding to maximum and minimum absorption points of the wavelength spectrum (Figure 4a). In the case of maximum absorption ($\lambda = 2190nm$), most of the power is dissipated into the top Au layer (50.45%). GST absorbs only 37.81 % of the incident power and the remaining power is absorbed in the Au mirror, confirming that the absorption mechanism is different from that of the broadband case. At the dip wavelength, both the GST and the bottom layers start to slightly absorb. Note that the graphs

represent only the fraction of the power absorbed in each layer and not its absolute value. This means that the increase in absorption compared to the case of Figure 4b is only apparent as one has to consider that the absorption in GST is negligible at this wavelength (1760 nm). Finally, in the case of the peak at 1160 nm, a relatively higher fraction of the light is absorbed in the GST layer, where GST has a higher loss.

Finally, a comparison with previous perfect absorber designs reported in the literature is shown in **Table 1**. The proposed structure has significant improvements in the visible in terms of absorption bandwidth and angular dependence. The fabrication techniques is another significant advantage over previous metamaterial and plasmonic antenna based absorbing surfaces, as it does not involve expensive lithography. Moreover our design using only few-layer structures can also be tailored for broadband or narrow band resonant operation, depending on the wavelength range and the structure design, thanks to the GST wavelength dependent absorption and refractive index coefficients.

In conclusion we have proposed and demonstrated a novel few-layer perfect optical absorbers incorporating phase change materials preventing from expensive and time consuming sophisticated lithography procedures. Thanks to their reliability, wavelength tailoring and optical response switching the proposed structures may be used to offer new functionalities, while plainness of deposition process makes such structures compatible with photovoltaic and photodetector technologies.

*Experimental Section*

*Sample fabrication:* The broadband perfect absorber samples were fabricated using RF sputtering and electron beam assisted evaporation techniques. The sample fabrication began by depositing the bottom mirror. Both the Ni and Au mirrors were deposited on top of fused silica

substrates by an electron beam assisted evaporation method. In the Au mirror case an initial 3 nm Ti layer had been previously deposited with the same method in order to enhance the adhesion of the Au film with the silica substrate. Then a 20 nm $SiO_2$ layer was deposited using an atomic layer deposition (ALD) system. This was followed by GST layer deposition using RF co-sputtering from two stoichiometric targets of GeTe and $Sb_2Te_3$ at 3.75 mT background pressure and 10 sccm Ar flow. The GST deposition rate was checked and carefully controlled by depositing samples of different thicknesses and measuring their thicknesses in an atomic force microscope (AFM). We used rotatable sample holder to maintain the thickness uniformity over the whole area of the samples. Finally the 60 nm $SiO_2$ layer was deposited to protect the GST layer and further reduce the reflection of the sample.

In the case of the narrowband absorber the first three layers are deposited using the same procedure, changing only the deposition times to get the appropriate thicknesses, and the top Au/Ni layer is deposited again using electron beam assisted evaporation.

*Reflection measurements:* Angle dependent reflection measurements of the samples were obtained using a commercial UV/vis/NIR spectrophotometer (Lambda900, Perkin Elmer) with a wavelength range between $\lambda = 300$ nm and $\lambda = 3300$ nm, using steps of 5 nm.

*Simulation methods*: All simulations were done using a transfer matrix method implemented in a python environment. Additional simulations were carried out using a genetic algorithm written in Matlab to generate different structures which show strong absorption. The fact that different combinations of metal-dielectric or semiconductor-dielectric layers can have similar performance in terms of absorption confirms that structures based on metal dielectric layers are well suited for this kind of applications.

*Acknowledgements*

We acknowledge financial support from Fundació Privada Cellex, AGAUR 2014 SGR 1623, the Spanish Ministry of Economy and Competitiveness (MINECO), through the "Severo

Ochoa" Programme for Centres of Excellence in R&D (SEV-2015-0522) and the "Fondo Europeo de Desarrollo Regional" (FEDER) through grant TEC2013-46168-R". J. C.-F. also thanks MINECO for his research grant funded by means of the program Juan de la Cierva (FPDI-2013-18078).

Received: ((will be filled in by the editorial staff))
Revised: ((will be filled in by the editorial staff))
Published online: ((will be filled in by the editorial staff))

[1] N. Landy, S. Sajuyigbe, J. Mock, D. Smith, W. Padilla, *Phys. Rev. Lett.* **2008**, 100, 207402.

[2] X. Xiong, S.-C. Jiang, Y.-H. Hu, R.-W. Peng, M. Wang, *Adv. Mater.* **2013**, 25, 3994.

[3] R. Feng, W. Ding, L. Liu, L. Chen, J. Qiu, G. Chen, *Opt. Express.* **2014**, 22, 335.

[4] J. Liu, M. Zhu, N. Zhang, H. Zhang, Y. Zhou, S. Sun, N. Yi, S. Gao, Q. Song, S. Xiao, *Nanoscale* **2015**, 7, 18914.

[5] X. Duan, S. Chen, W. Liu, H. Cheng, Z. Li, J. Tian, *J. Opt.* **2014**, 16, 125107.

[6] J. Rhee, Y. Yoo, K. Kim, Y. Kim, Y. Lee, *J. Electromagnet. Wave.* **2014**, 28, 1541.

[7] J. Wang, C. Fan, P. Ding, J. He, Y. Cheng, W. Hu, G. Cai, E. Liang, Q. Xue, *Opt. Express* **2012**, 20, 14871.

[8] Z. Li, S. Butun, K. Aydin, *ACS Photonics* **2015**, 2, 183.

[9] S. Butun, K. Aydin, *Opt. Express* **2014**, 22, 19457.

[10] Y. Ra'di, C. Simovski, S. Tretyakov, *Phys. Rev. Applied* **2015**, 3, 037001.

[11] Z. Li, E. Palacios, S. Butun, H. Kocer, K. Aydin, *Sci. Rep.* **2015**, 5.

[12] H. Deng, Z. Li, L. Stan, D. Rosenmann, D. Czaplewski, J. Gao, X. Yang, *Opt. Lett.* **2015**, 40, 2592.

[13] M. Yan, *J. Opt.* **2013**, 15, 025006.

[14] T. D. Dao, K. Chen, S. Ishii, A. Ohi, T. Nabatame, M. Kitajima, T. Nagao, *ACS Photonics* **2015**, 2, 964.

[15] M. K. Hedayati, M. Javaherirahim, B. Mozooni, R. Abdelaziz, A. Tavassolizadeh, V.

S. K. Chakravadhanula, V. Zaporojtchenko, T. Strunkus, F. Faupel, M. Elbahri, *Adv. Mater.* **2011**, 23, 5410.

[16] M. K. Hedayati, F. Faupel, M. Elbahri, *Appl. Phys. A* **2012**, 109, 769.

[17] Z. Liu, X. Liu, S. Huang, P. Pan, J. Chen, G. Liu, G. Gu, *ACS Appl. Mater. Interfaces* **2015**, 7, 4962.

[18] M. A. Kats, D. Sharma, J. Lin, P. Genevet, R. Blanchard, Z. Yang, M. M. Qazilbash, D. Basov, S. Ramanathan, F. Capasso, *Appl. Phys. Lett.* **2012**, 101, 221101.

[19] M. A. Kats, S. J. Byrnes, R. Blanchard, M. Kolle, P. Genevet, J. Aizenberg, F. Capasso, *Appl. Phys. Lett.* **2013**, 103, 101104.

[20] M. A. Kats, R. Blanchard, P. Genevet, F. Capasso, *Nat.Mater.* **2013**, 12, 20.

[21] Z. Fang, Y. Wang, A. E. Schlather, Z. Liu, P. M. Ajayan, F. J. García De Abajo, P. Nordlander, X. Zhu, N. J. Halas, *Nano Lett.* **2014**, 14, 299.

[22] X. He, *Carbon* **2015**, 82, 229.

[23] M. K. Hedayati, M. Javaheri, A. U. Zillohu, H. J. El-Khozondar, M. S. Bawa'aneh, A. Lavrinenko, F. Faupel, M. Elbahri, *Adv. Opt. Mater.* **2014**, 2, 705.

[24] P. Hosseini, C. D. Wright, H. Bhaskaran, *Nature* **2014**, 511, 206.

[25] M. A. Kats, R. Blanchard, P. Genevet, Z. Yang, M. M. Qazilbash, D. Basov, S. Ramanathan, F. Capasso, *Opt. Lett.* **2013**, 38, 368.

[26] M. Rudé, R. E. Simpson, R. Quidant, V. Pruneri, J. Renger, *ACS Photonics* **2015**, 2, 669.

[27] Y. Chen, T. Kao, B. Ng, X. Li, X. Luo, B. Luk'yanchuk, S. Maier, M. Hong, *Opt. Express* **2013**, 21, 13691.

[28] M. Rudé, J. Pello, R. E. Simpson, J. Osmond, G. Roelkens, J. J. van der Tol, V. Pruneri, *Appl. Phys. Lett.* **2013**, 103, 141119.

[29] M. Rudé, V. Mkhitaryan, A. E. Cetin, T. A. Miller, A. Carrilero, S. Wall, F. J. G. de Abajo, H. Altug, V. Pruneri, *arXiv:1506.03739*, **2015**.

[30] A. Tittl, A.-K. U. Michel, M. Schaferling, X. Yin, B. Gholipour, L. Cui, M. Wuttig, T. Taubner, F. Neubrech, H. Giessen, *Adv. Mater.* **2015**, 27, 4597.

[31] T. Cao, C. Wei, R. E. Simpson, L. Zhang, M. J. Cryan, *Opt. Mater. Express* **2013**, 3, 1101.

[32] T. Cao, C. Wei, R. E. Simpson, L. Zhang, M. J. Cryan, *Sci. Rep.* **2014**, 4.

[33] Y. Chen, X. Li, X. Luo, S. A. Maier, M. Hong, *Photon. Res.* **2015**, 3, 54.

[34] Y. Cui, J. Xu, K. H. Fung, Y. Jin, A. Kumar, S. He, N. X. Fang, *Appl. Phys. Lett.* **2011**, 99, 253101.

[35] H. Song, L. Guo, Z. Liu, K. Liu, X. Zeng, D. Ji, N. Zhang, H. Hu, S. Jiang, Q. Gan, *Adv. Mater.* **2014**, 26, 2737.

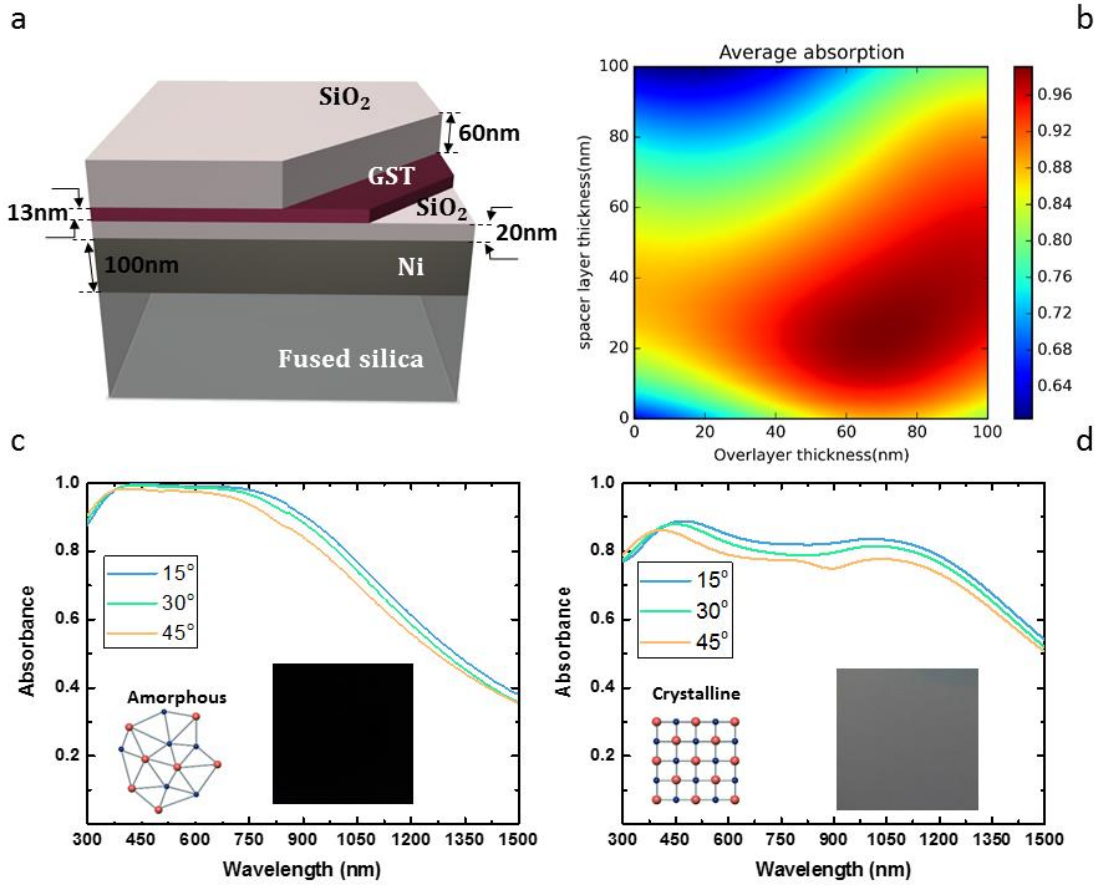


**Figure 1.** a) 3D sketch of the proposed structure. b) Spacer and overlayer thickness dependence of the angle and wavelength averaged absorption. c),d) Experimental absorption curves for three different incidence angle for amorphous and crystalline phase, respectively. c), d) Inset: real image of the fabricated samples correspondingly in amorphous and crystalline phase.

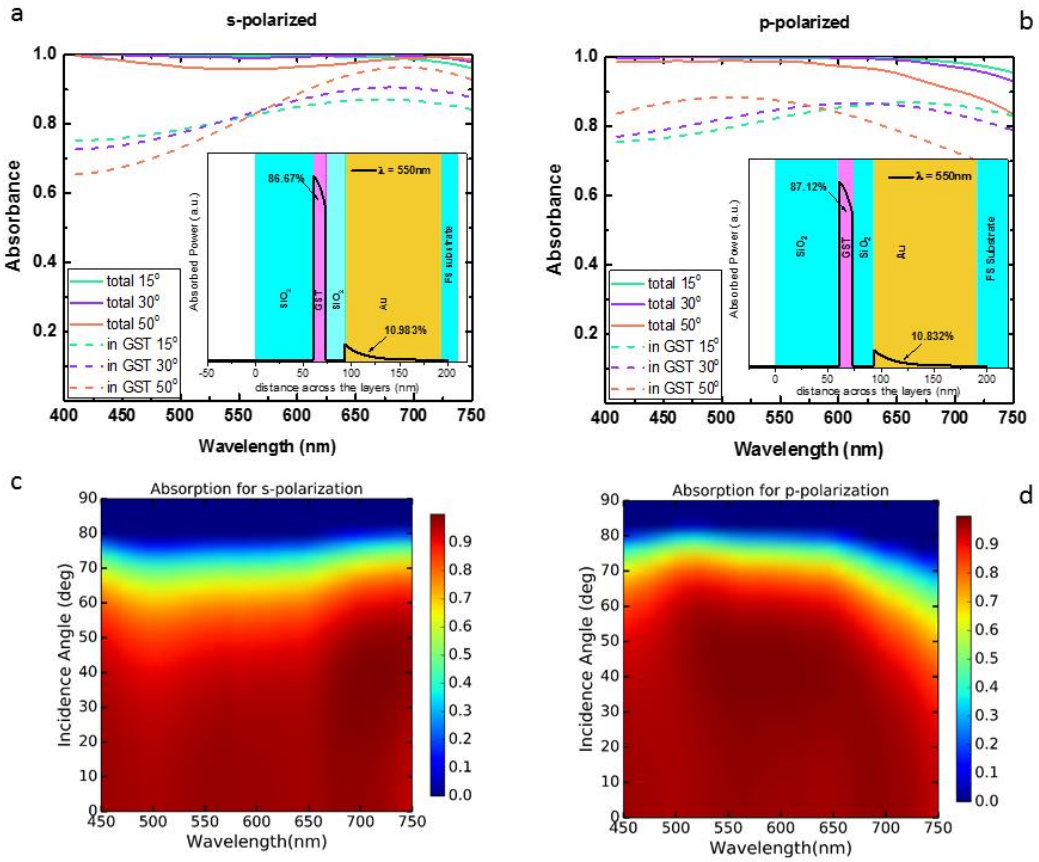


**Figure 2.** a) Comparison of the total absorption and the absorption in GST layer for different incidence angles in the case of s-polarized incidence light. b) Same comparison in the case of p-polarization. a), b) Insets: angle and wavelength dependent absorption for s and p-polarized incident light.

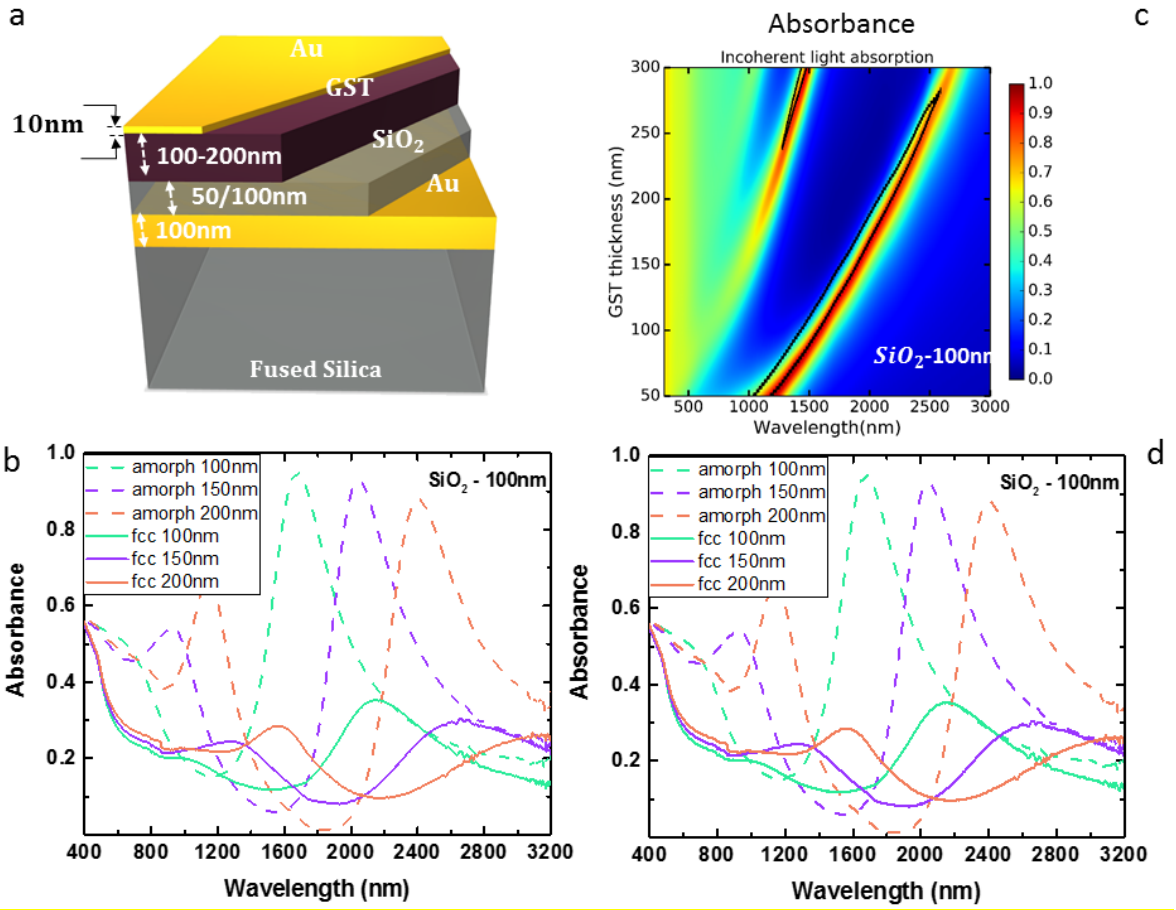


**Figure 3.** a) 3D sketch of the narrowband absorber. b) Colormap plot of the simulation results for device absorption for 100nm thick $SiO_2$ layer and GST thicknesses in the range of 50-300nm. The black contour line represents the contour of the region where the phase and amplitude balance equations are satisfied. c) Experimental absorption curves for unpolarized light for 50 nm $SiO_2$ spacer layer, amorphous and crystalline GST layers. d) Absorption of the same structure with a thicker $SiO_2$ spacer layer (100 nm).

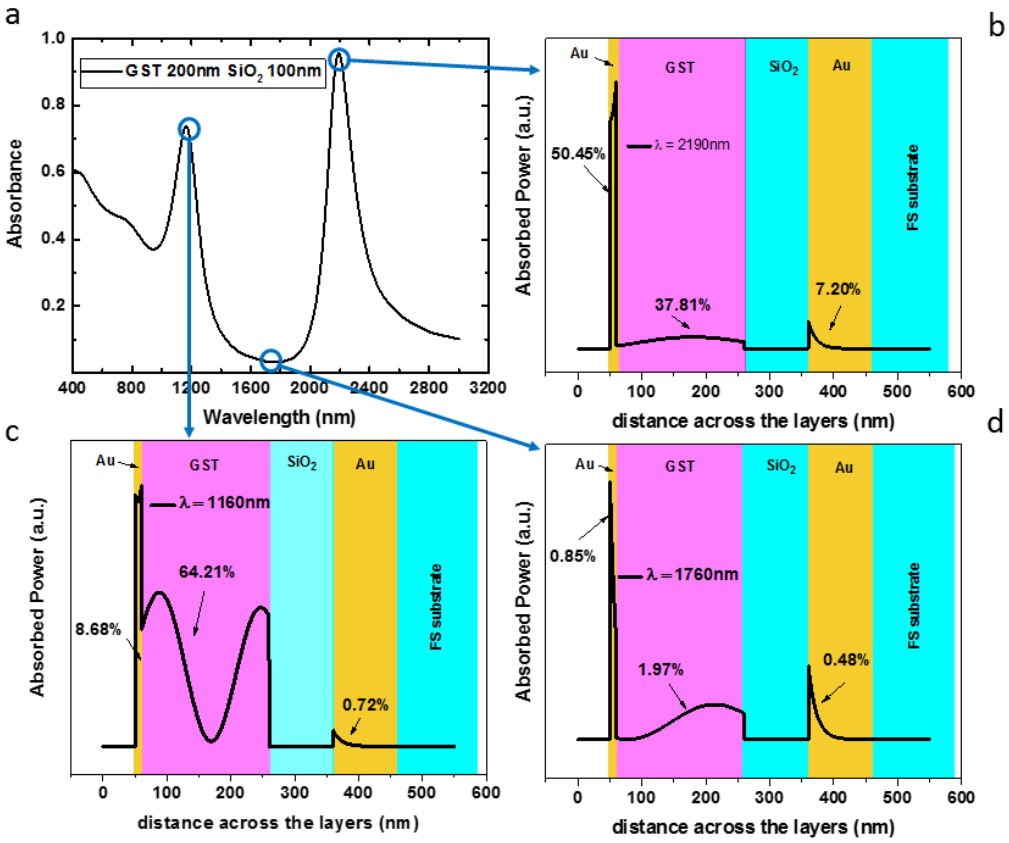


**Figure 4.** a) Simulated wavelength dependent absorbance for resonant structure with 200 nm thick GST and 100 nm thick $SiO_2$. b), c), d) Absorption profiles across the multilayer structure at $\lambda = 2190\ nm$, $\lambda = 1160\ nm$ and $\lambda = 1760\ nm$ respectively.

**Table 1.** Comparison with previously demonstrated optical absorbers.

| | Wavelength range [um] | Polarization independence | Wide angle | Total abs | Abs in active layer | Lithography free | Dynamic Tunability |
|---|---|---|---|---|---|---|---|
| This work | 0.3 - 0.8 NIR-resonant | yes | yes | ~100% | up to 85% in vis and 95% in NIR | yes | yes |
| N. Liu et al. Nano Lett. 2010, 10, 2342–2348 | 1.3 - 2.1 | yes | no | ~100% | --- | no | no |
| H. Song et al. Adv. Mater. 2011, 23, 5410 –5414 | 0.4 - 1 | yes | yes | ~100% | 20-80% | yes | no |
| M. K. Hedayati et al. Appl Phys A 2012, 109, 769–773 | 0.3- 0.8 | --- | --- | 80% to >95% | --- | yes | no |
| M. K. Hedayati et al. Adv. Mater. 2011, 23, 5410–5414 | 0.4 - 0.75 | no | yes | >95% | --- | yes | no |
| Z. Li et al. ACS Photonics 2015, 2, 183−188 | visible-resonant | no | no | 90-95% | no | yes | no |
| M. A. Kats et al. Appl. Phys. Lett. 2012, 101, 221101 | 2-10 | --- | --- | 20-80% | --- | no | yes |
| A. Tittle et al. Adv. Mater. 2015, 27, 4597–4603 | 2.5 - 4 | yes | yes | 90% | --- | no | yes |
| T. Cao et al. Scientific Reports 2014, 4 , 3955 | 0.61 – 0.87 | yes | yes | >95% | --- | no | yes |
| Y. Chen et al. 2015 Chinese Laser Press | 1 - 3 | no | --- | ~100% | --- | no | yes |
| M. K. Hedayati et al. Appl. Phys. Lett. 2014, 104, 041103 | 0.35-0.55 | no | yes | ~100% | --- | yes | no |

**The table of contents entry** should be fifty to sixty words long, written in the present tense, and refer to the chosen figure.

Keyword (see list)

*Vahagn K. Mkhitaryan, Dhriti S. Ghosh, Miquel Rudé, Josep Canet-Ferrer, Rinu Abraham Maniyara, Kavitha K. Gopalan and Valerio Pruneri**

Broadband and resonant perfect optical absorption in multilayer structures without lithographic patterns

ToC figure ((55 mm broad, 50 mm high, or 110 mm broad, 20 mm high))